Supplemental Figures and Figure Legends

Note that full statistics information is provided in the Supplemental Statistics Table S7.

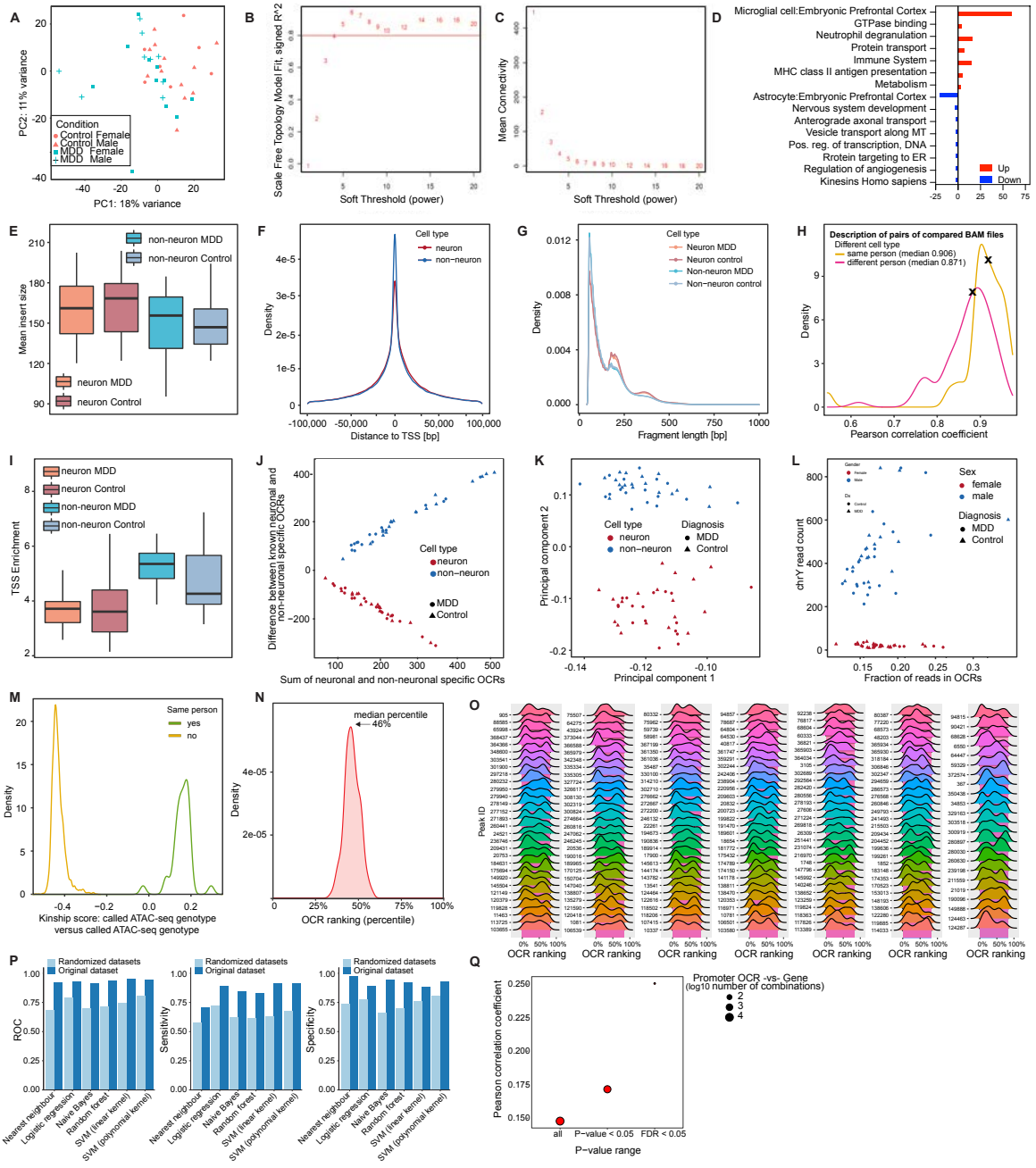

Supplemental Figure 1. Quality control metrics for human postmortem MDD molecular profiling.

(**A**) Principal component analysis of sample gene expression levels. (**B**) Analysis of scale-free fit index for possible soft-thresholding powers (β). (**C**) Analysis of mean connectivity for possible soft-thresholding powers. (**D**) GO analysis for 1,450 DE genes between MDD and control groups, separated by up/down regulation. (**E**) Fraction of uniquely mapped, non-duplicated, non-chrM paired-end reads compared to all reads in raw sequencing files. (**F**) Number of uniquely mapped, non-duplicated, non-chrM paired-end reads. (**G**) Fraction of duplicated to uniquely mapped paired-end reads. (**H**) Fraction of mitochondrial DNA reads to uniquely mapped, non-duplicated paired-end reads. (**I**) Number of OCRs (called per sample). (**J**) Fraction of reads in OCRs (FRiP). (**K**) GC-content in consensus set of OCRs; (**L**) Median insert size. For all whisker plots in this figure: The center line indicates the median, the box shows the interquartile range, whiskers indicate the highest/lowest values within 1.5x the interquartile range. (**M**) Genotype check based on pair-wise comparison of genotypes called from ATAC-seq samples. Pairs of neuronal and non-neuronal samples supposedly originating from the same person have distinctly higher scores (green line) than pairs of samples from different individuals (yellow line). (**N**) Summary and (**O**) per-OCR distribution of *P*-value ranking for the reported set of 203 differentially accessible OCRs within differentially analyses results generated on the datasets of non-neuronal samples with randomly permuted MDD and Control status (n=100 permuted datasets). This analysis proves that the reported set of 203 differentially accessible OCRs (median percentile of *P*-value is 1%) are not affected by technical artifacts since their median percentile of *P*-value in the datasets with permuted MDD and Control status is 46% (further details in Methods: Differential analysis of chromatin accessibility). (**P**) Performance of machine learning classifiers built on the reported set of 203 differential OCRs and 203 random OCRs. To enable the robust performance evaluation, the repeated 5-fold cross-validation was applied ($k_{repeat} = 10$); additionally, the whole process was repeated 10 times with different sets of 203 randomly selected OCRs. For all whisker plots in this figure: The center line indicates the median, the box shows the interquartile range, whiskers indicate the highest/lowest values within 1.5x the interquartile range. Student's two-tailed t-tests were performed for statistical comparisons, *=p<.05, **=p<.01. Data displayed as mean (+/- SEM).

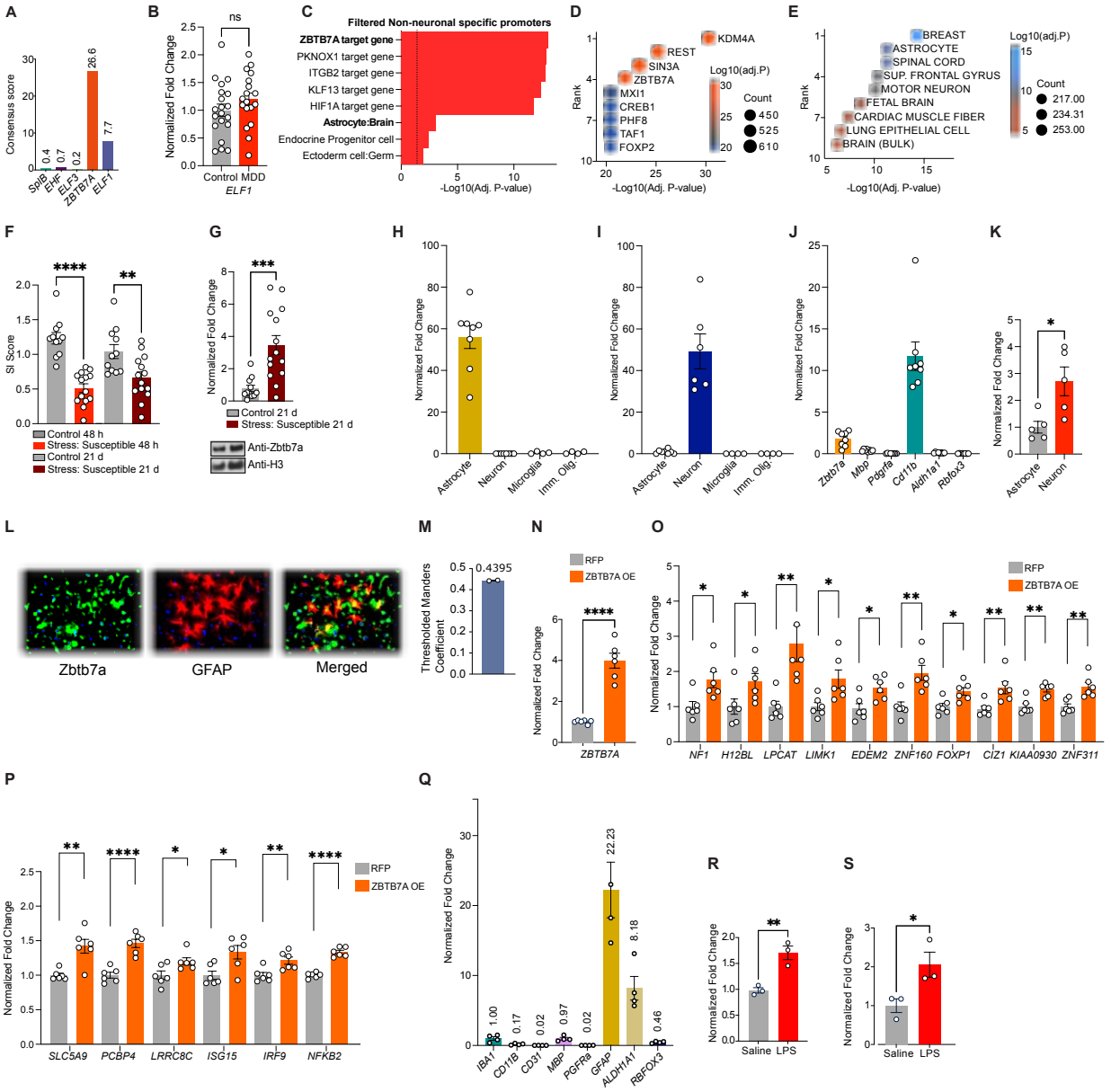

Supplemental Figure 2. Identification and characterization of ZBTB7A in human MDD and mouse chronic stress OFC.

(**A**) Consensus score from the Human Protein Atlas[1] for expression in human brain for each factor. The mRNA expression data is derived from deep sequencing of RNA (RNA-seq) from 37 different normal tissue types. (**B**) Normalized fold change for mRNA expression for ELF1 in bulk human OFC tissues, control *vs.* MDD. (**C**) GO analysis with CellMarker Augmented Database[2] and CHEA ENCODE Consensus database[3] for genes in detected non-neuronal specific promoters, filtered by logFC > 1, (+/-) 3000bp from TSS (**D**) Overlap between DE genes from MDD *vs.* control OFC tissues[4] and ENCODE consensus target gene sets via EnrichR, plotted by rank (y-axis) and -

log_{10}(adjusted *p*-value) on the x-axis and by fill color. Bubble size displays the number of overlapping genes for each term. (**E**) Overlap between ZBTB7A target genes (from TRANSFAC) and ARCHS4 human tissue expression reference gene sets via EnrichR. plotted by rank (y-axis) and -log_{10}(Adjusted P-value) on the x-axis and by fill color. Bubble size displays the number of overlapping genes for each term. (**F**) Social interaction ratio for control vs. chronically stressed CSDS mouse groups at 48 h post-stress and 21 d post-stress. (**G**) Normalized fold change protein expression of Zbtb7a in mouse OFC bulk tissues collected from control vs. chronically stressed mouse groups at 21 d post-stress. (**H**) qPCR expression data for astrocyte-specific gene *Aldh1a1* in MACs-isolated cell fractions (**I**) qPCR expression data for neuron-specific *Rbfox3* (*NeuN* in MACs-isolated cell fractions). (**J**) qPCR expression data for cell type-specific genes in negative fraction from MACs-isolated astrocyte and neuron cell fractions, showing the negative fraction is enriched for microglia marker *Cd11b*. (**K**) qPCR expression data for *Zbtb7a* in MACs-isolated astrocyte vs. neuron cell fractions. (**L**) 20x IHC images showing Zbtb7a protein is expressed in mouse OFC astrocytes, depicts overlap of Zbtb7a with astrocyte-specific marker Gfap. (**M**) Thresholded Mander's coefficient describes overlap of color channels of interest. (**N**) Expression of *ZBTB7A* mRNA in human primary cultured astrocytes treated with *ZBTB7A* OE lentivirus *vs.* RFP empty vector control virus. (**O-P**) Bar graph showing normalized fold change of mRNA expression in ZBT-OE vs. RFP human primary cultured astrocytes for the listed gene targets. (**Q**) Normalized fold change of cell-type specific marker genes in human primary astrocyte-enriched cultures. (**R**) Normalized fold change of *ZBTB7A* mRNA expression in cultured human astrocytes treated with saline vs. LPS. (**S**) Normalized fold change of *Zbtb7a* mRNA expression in cultured mouse astrocytes treated with saline vs. LPS. Student's two-tailed t-tests or 1-way ANOVA with MC tests were performed for statistical comparisons. Data presented as mean (+/- SEM). *=p<.05, **=p<.01, ***=p<.001, ****=p<.0001.

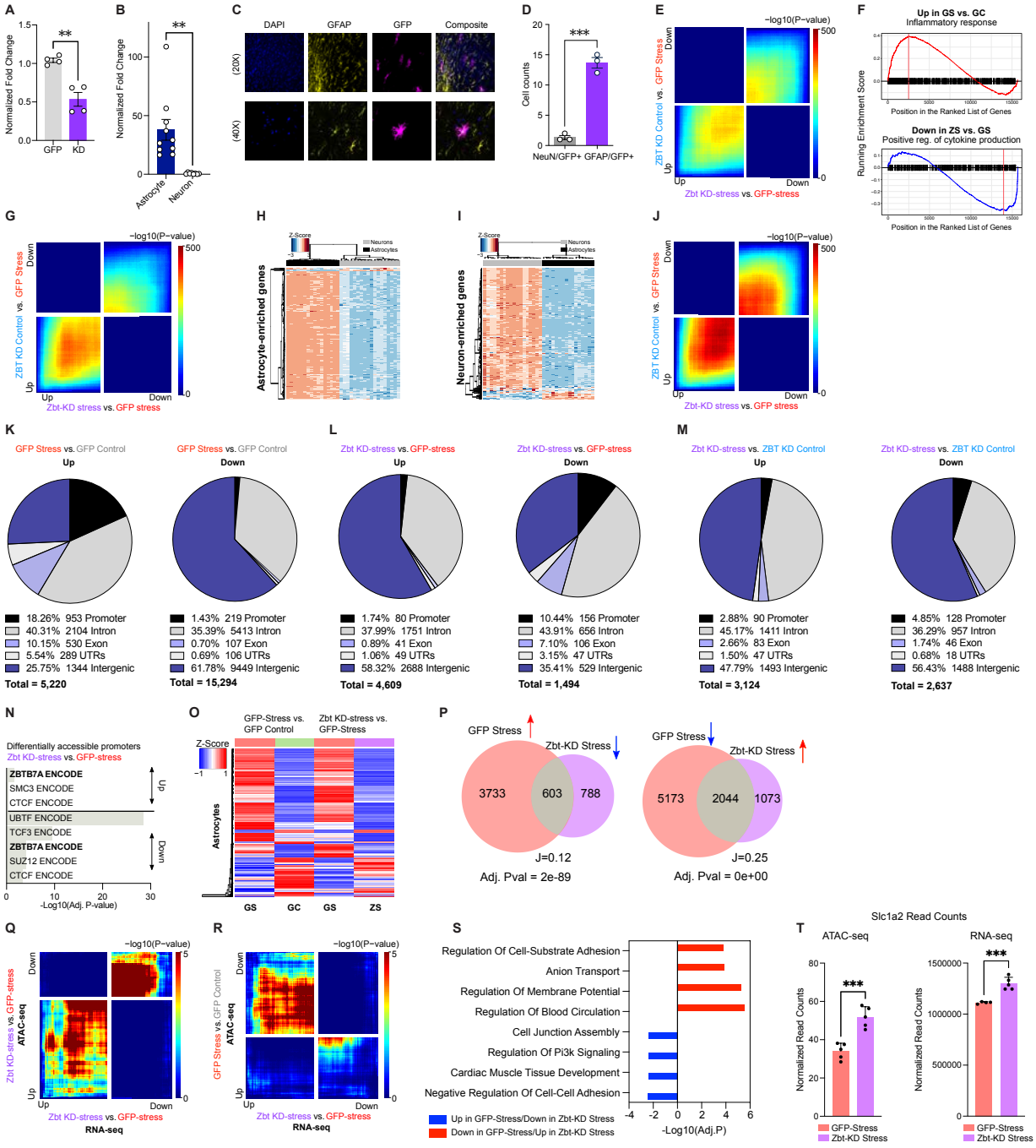

Supplemental Figure 3. Zbtb7a KD alters cell-type specific chromatin accessibility and gene expression.

(**A**) Normalized fold change of qPCR *Zbtb7a* gene expression from OFC tissues transduced with Zbt-KD virus vs. miR-neg-GFP (GFP), with n = 4/group. (**B**) qPCR expression levels of the GFP transgene in MACs-isolated neurons vs. astrocytes from AAV6-GFAP-miR-neg-GFP virally-transduced OFC mouse tissues. (**C**) Representative IHC images of OFC tissues transduced with an rAAV6 virus expressing ZBTB7A-GFP (in magenta) overlaid with a nuclear co-stain (DAPI in

blue) and GFAP (in yellow) to show astrocyte-specific expression. (**D**) Cell counts in OFC tissues transduced with AAV6-ZBTB7A-GFP of cells co-expressing Gfap/Zbtb7a or NeuN/Zbtb7a. (**E**) RRHO comparing gene expression for the indicated comparisons, in bulk OFC tissue. (**F**) GSEA enrichment plot for most significantly enriched gene set in GFP Stress vs. GFP Control and ZBT stress vs. GFP Stress in bulk OFC tissue. The enrichment plot shows a line representing the running ES for a given GO as the analysis goes down the ranked list. The value at the peak is the final ES. (**G**) RRHO comparing gene expression for the indicated comparisons, in MACS-isolated astrocytes. (**H-I**) Heatmaps depict unsupervised clustering of normalized read count values in MACs-isolated astrocytes and neurons for (H) 239 astrocyte-enriched genes and (I) 279 neuron enriched genes identified in previous report[5]. (**J**) RRHO comparing gene expression for the indicated comparisons, in MACS-isolated neurons. (**K-M**) ATAC-seq diffReps analysis of differential accessibility between indicated conditions. Pie charts indicate distribution of differential accessibility events, stratified by genomic context for the indicated conditions and separated for up/down events. (**N**) Gene ontology (GO) pathway analysis of differentially accessible promoters from Zbt-KD stress vs. GFP stress [less accessible promoters, top] and GFP stress vs. GFP control [more accessible promoters, bottom]. (**O**) Clustering of groups at 1,138 overlapping genomic regions between GFP Stress vs. GFP control and Zbt-KD stress vs. GFP stress, depicting Z-score of log2FC accessibility. (**P**) Scaled Venn diagram and odds ratio analyses of the number of shared and distinct OCR gene targets between indicated conditions. Numbers indicate differentially accessible peaks, "*J*" indicates the Jaccard index. (**Q-R**) RRHO comparing gene expression and chromatin accessibility for the indicated comparisons. (**S**) GO pathway analysis of rescued OCR gene targets between Zbt-KD Stress and GFP Stress MACS-isolated astrocytes ATAC-seq. (**T**) Normalized read counts for accessibility (left) and gene expression (right) at *Slc1a2* gene in MACS-isolated astrocytes. Data were analyzed with Student's two-tailed t-tests. *=p<.05, **=p<.01, ***=p<.001, ****=p<.0001. All data graphed as means ± SEM.

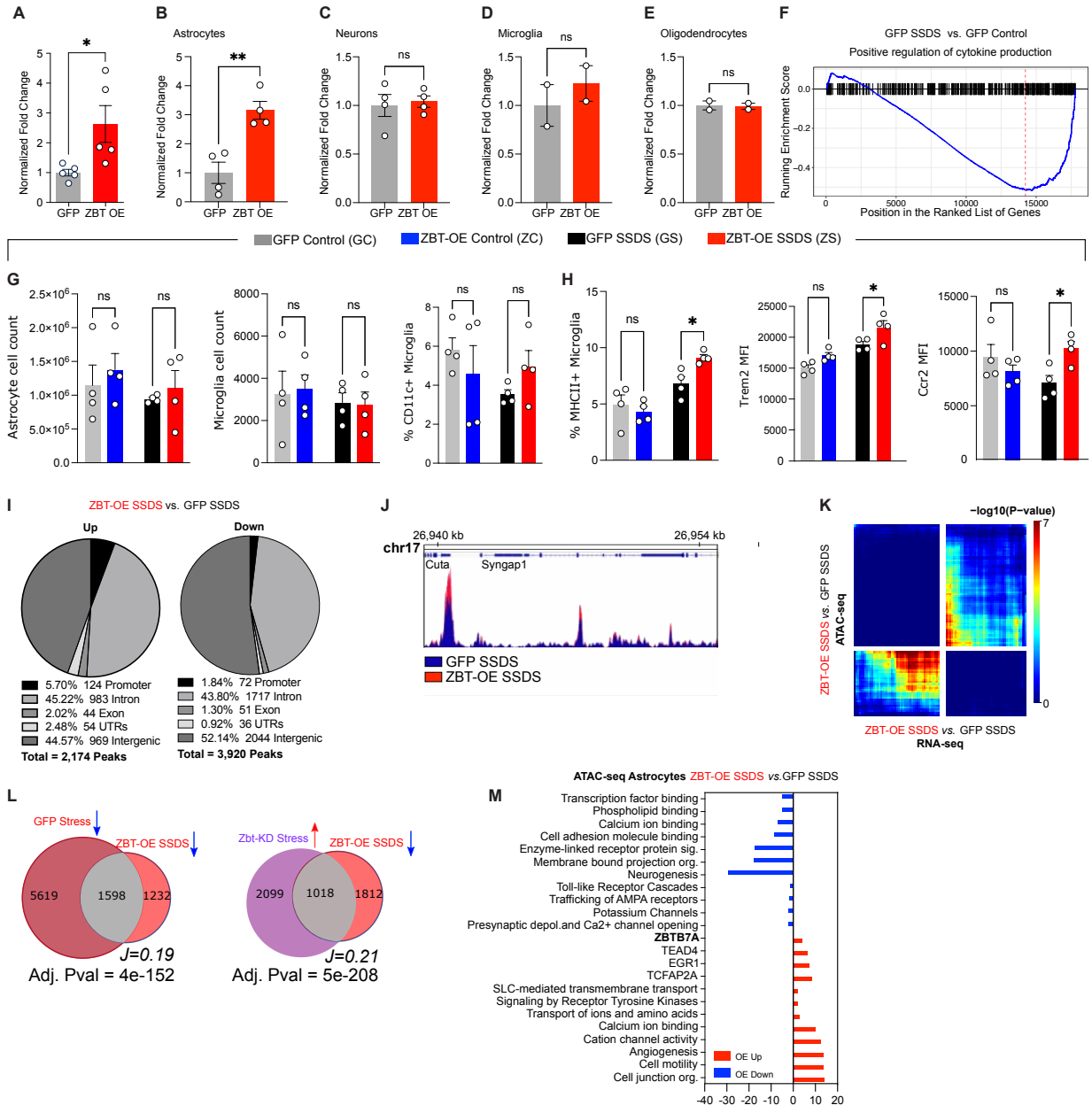

Supplementary Figure 4. ZBTB7A OE in OFC astrocytes promotes significant alterations in behavior, chromatin accessibility, and gene expression.

(**A**) Normalized fold change of qPCR *Zbtb7a* gene expression from OFC tissues transduced with ZBTB7A OE virus *vs.* GFP, n = 5/group. (**B-E**) qPCR expression levels of *Zbtb7a* in MACs-isolated (B) astrocytes and (C) neurons (D) microglia and (E) oligodendrocytes from AAV6-GFAP-ZBT OE transduced virally-transduced OFC mouse tissues, n = 2-4/group. (**F**) GSEA enrichment plot for most significantly enriched gene set in GFP Stress vs. GFP Control in bulk OFC tissue. (**G**) Number of astrocytes [left], and microglia[6] per organ. (**H**) Percent CD11c+ microglia [far left],

percent MHCII+ microglia [left], Trem2 MFI^6 and Ccr2 [far right] MFI^6 in virally transduced ZBT-OE vs. GFP mice (+/- SSDS) OFC via flow cytometry, n = 4/group. Gating strategy shown in **Supplementary Fig. 6.** (**I**) ATAC-seq diffReps analysis of differential accessibility comparing ZBT-OE SSDS vs. GFP SSDS. Pie charts indicate distribution of differential accessibility events, stratified by genomic context. (**J**) Representative pile-up traces of cell specific ATAC-seq signal overlapping Syngap1 gene. (**K**) RRHO comparing gene expression profile of MACs-isolated astrocytes with MACS-isolated astrocyte chromatin accessibility for indicated conditions. (**L**) Venn diagram and odds ratio analysis of the shared and distinct OCRs from ATAC-seq diffreps analysis between indicated conditions. (**M**) GO pathway analysis of gene targets associated with differentially expressed [red is more accessible, blue is less accessible] chromatin regions between ZBT-OE SSDS and GFP OE SSDS. Data were analyzed with Student's two-tailed t-tests or with 2-way ANOVA, or 3-way ANOVA, followed by 2-Way ANOVAs for MC comparisons, *=p<.05, **=p<.01. All data graphed as means ± SEM.

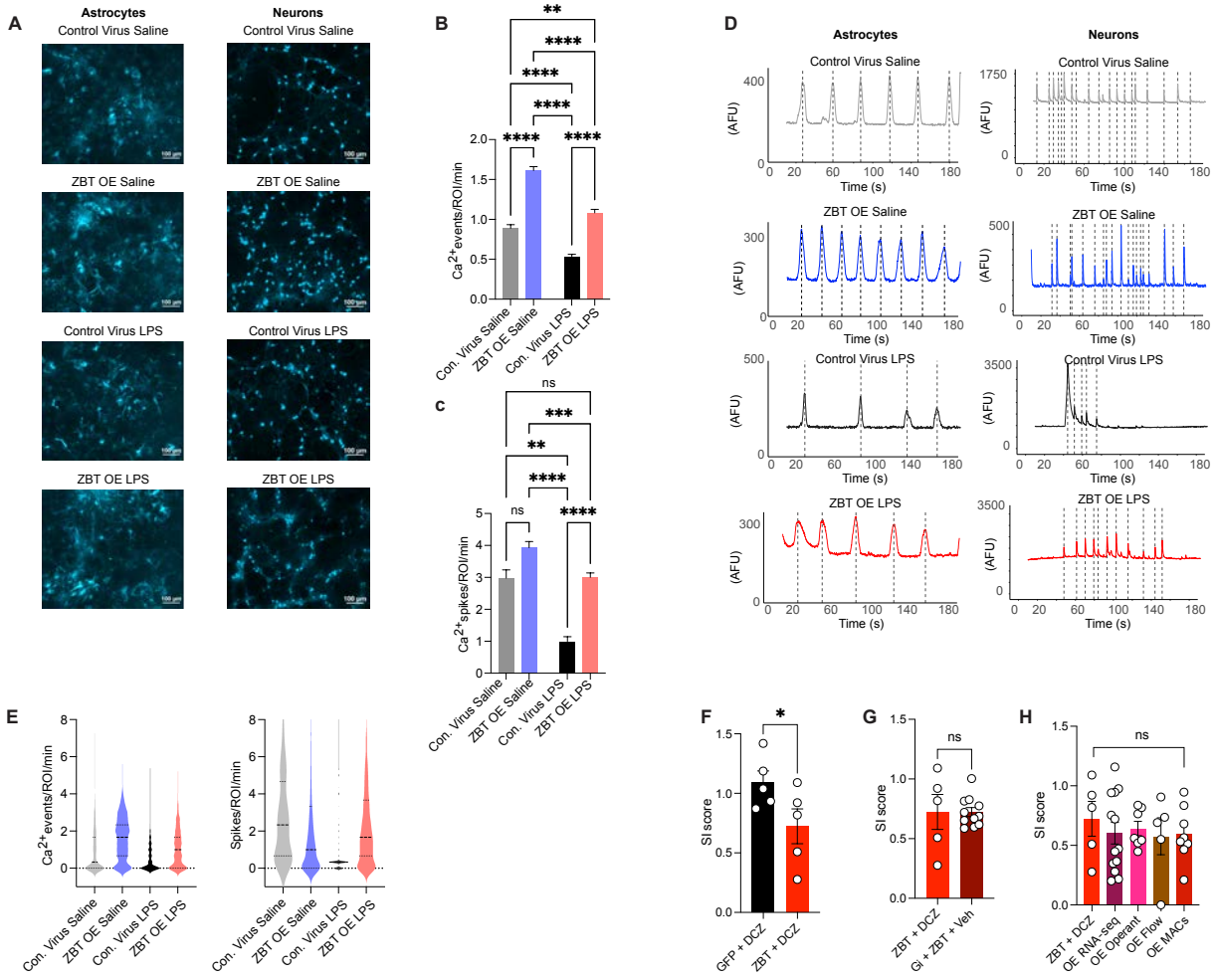

Supplemental Figure 5. Calcium imaging and chemogenetic manipulations in the context of astrocyte-specific ZBT7A OE.

(**A**) Representative images show gCAMP6f-expressing cells in either astrocyte-treated or neuron-treated primary co-cultures. (**B**) Mean frequency of Ca2+ events detected in astrocytes expressing gCAMPf. “Con.” Indicates Control. Representative traces show (**C**) Mean frequency of Ca2+ event detected in neurons expressing gCAMP6f. “Con.” Indicates Control. (**D**) Representative traces for calcium event frequencies in astrocytes [left] and neurons[6]. (**E**) Violin plots depicting individual values for (right) astrocyte [*n*=623 cells control virus saline, *n*= 559 cells ZBT-OE saline, *n*=747 cells control virus LPS, and *n*=517 cells ZBT-OE LPS] and (left) neuronal [*n*=135 cells control virus saline, *n*= 1277 cells ZBT-OE saline, *n*=238 cells control virus LPS, and *n*=1324 cells ZBT OE LPS] calcium events. (**F**) Social interaction score for ZBT OE SSDS vs. GFP SSDS mice injected with DCZ. (**G**) Social interaction score for ZBT-OE SSDS vs. ZBT-OE + G_i Dreadd + vehicle. (**H**) Comparison of SI score across multiple cohorts of ZBT-OE SSDS

1921 animals. Data were analyzed with Student's two-tailed t-tests or with 1-way ANOVA plus Tukey's
1922 MC test, *=p<.05, **=p<.01, ***=p<.001, ****=p<.0001. All data graphed as means ± SEM.
1923

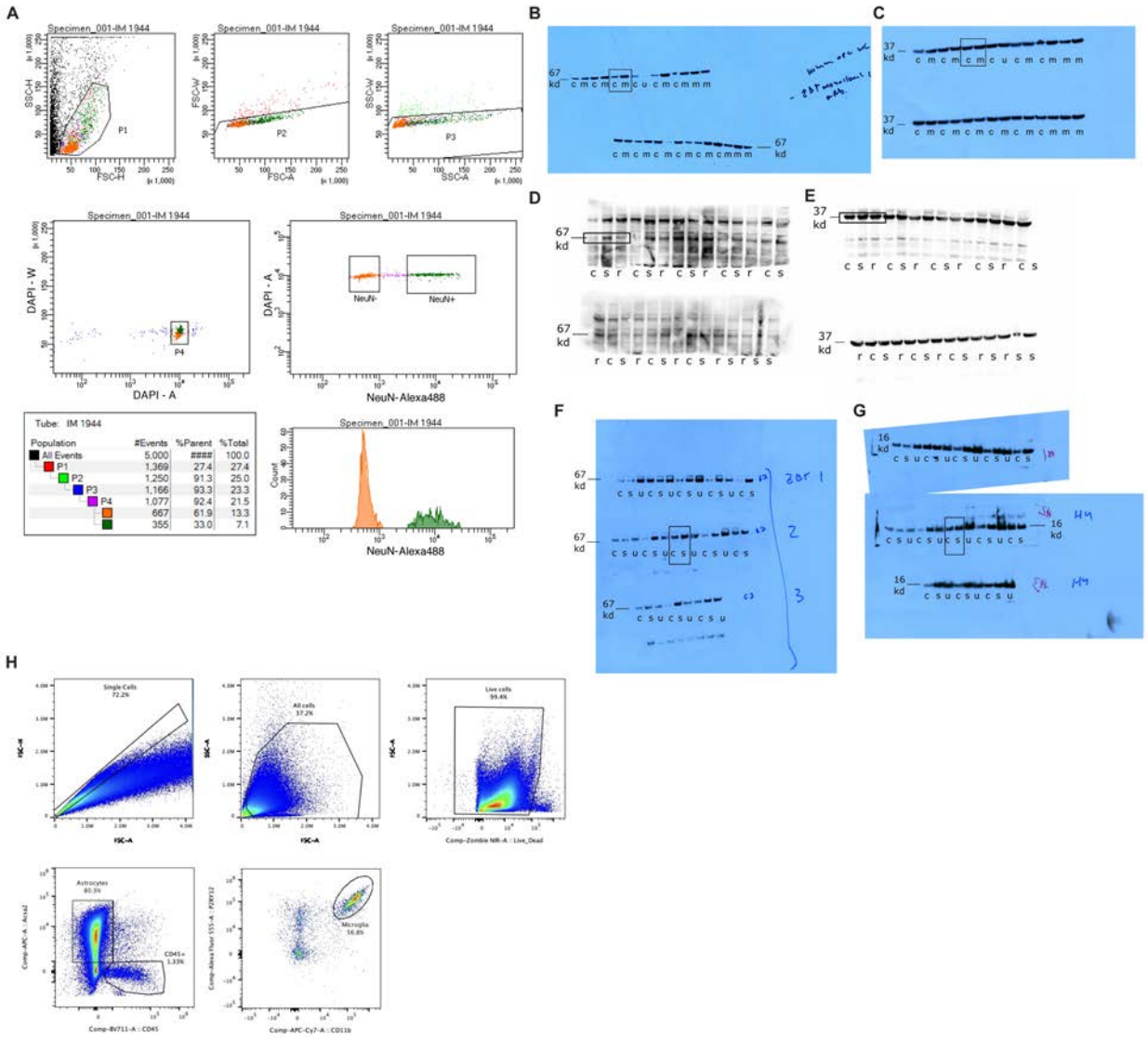

Supplemental Figure 6. Flow cytometry gating and raw blots

(**A**) For FANS-coupled ATAC-seq on human postmortem tissues, nuclear populations were initially gated by side and forward scatter to differentiate nuclei from cellular debris. Populations were then gated based on DAPI staining to identify singlets and to further disregard debris. DAPI positive nuclei were subsequently gated based on NeuN staining to differentiate neurons ($NeuN^+$) from non-neurons ($NeuN^-$). Final nuclei population abundance for non-Neurons ($NeuN^-$): 70.5% (in orange) and for neurons ($NeuN^+$): 29.5% (in green). (**B**) Western blot film scan for ZBTB7A in bulk human OFC tissue, MDD (labeled “m”) vs. controls (labeled “c”). ZBTB7A band at expected molecular weight of 67kDa. Note samples labeled “u” are not included in this manuscript due to lack of signal (suspected improper nuclear lysis). (**C**) Western blot film scan for housekeeping

gene GAPDH in human OFC, MDD vs. controls. Run on the same membrane as ZBTB7A in (B). (**D**) Raw image from chemidoc for western blot film for Zbtb7a in male mouse OFC, 48 hours after final defeat. CSDS susceptible (labeled “s”) vs. CSDS resilient (labeled “r”) vs. controls (labeled “c”). (**E**) Raw image from chemidoc western blot film for Gapdh loading control in male mouse OFC, CSDS susceptible vs. resilient vs. controls. Run on the same membrane as Zbtb7a in (D). (**F**) Western blot film scan for Zbtb7a in male mouse OFC, 21 days after final defeat. CSDS susceptible (labeled “s”) vs. controls (labeled “c”). Note samples labeled “u” are from an unrelated study, and not included in this manuscript. (**G**) Western blot film scan for H3.3 loading control in male mouse OFC, CSDS susceptible *vs.* controls (note H3.3 was used for these blots due to use of nuclear lysates, Gapdh could not be used). Run on the same membrane as Zbtb7a in (F). (**H**) Gating strategy used to identify cell populations in the OFC of mouse OE experiments (Fig. S4).

Supplemental References

1 Uhlén, M. *et al.* Tissue-based map of the human proteome. *Science* **347** (2015).

2 Zhang, X. *et al.* CellMarker: a manually curated resource of cell markers in human and mouse. *Nucleic acids research* **47**, D721-D728 (2019).

3 Lachmann, A. *et al.* ChEA: transcription factor regulation inferred from integrating genome-wide ChIP-X experiments. *Bioinformatics* **26**, 2438-2444 (2010).

4 Labonté, B. *et al.* Sex-specific transcriptional signatures in human depression. *Nature medicine* **23**, 1102 (2017).

5 McKenzie, A. T. *et al.* Brain cell type specific gene expression and co-expression network architectures. *Scientific reports* **8**, 1-19 (2018).

6 Wright, C. F. *et al.* Making new genetic diagnoses with old data: iterative reanalysis and reporting from genome-wide data in 1,133 families with developmental disorders. *Genetics in Medicine* **20**, 1216-1223 (2018).